Research Square

Preprints are preliminary reports that have not undergone peer review.
They should not be considered conclusive, used to inform clinical practice,
or referenced by the media as validated information.

In-silico design of Phosphorus-doped endohedral fullerenes ($Sc_3P@C_{80}$) as sensors for anticancer drug: A DFT study of Metformin (MFM) adsorption

Lubem Aondoakaa

aondoakaa89lubem@gmail.com

University of Calabar

David John

Modibbo Adama University

Chukwuebuka E. Mgbemere

Federal University of Technology Owerri

Omobolanle Rofiat Savage

University of Cross River State

Musa Runde

National Open University of Nigeria

Article

Keywords: Adsorption, Anticancer, Fullerene, DFT, Metal-complex

Posted Date: April 29th, 2026

DOI: https://doi.org/10.21203/rs.3.rs-9089168/v1

License: This work is licensed under a Creative Commons Attribution 4.0 International License.
Read Full License

Additional Declarations: No competing interests reported.

Abstract

A thorough density functional theory (DFT) study of $Sc_3P@C_{80}$ and its doped models (Fe, Os, and Ru) is carried out in this work at the PBE-D3/Def2-SVP level of calculations. Spin stability showed that all the pristine and metal-doped $Sc_3P@C_{79}$ systems favour a septet ground state, which indicates a high degree of spin polarization that is formed as a result of interaction between the Sc_3P cluster encapsulated, and the fullerene cage. The structural analysis indicates that $Sc_3P@C_{80}$ has an energy gap of 2.499 eV, which reduces slightly to 2.470 eV on metformin adsorption. Transition-metal doping accelerates the electronic activity by lowering band gaps to about 2.012 eV, with Os-$Sc_3P@C_{79}$ showing the lowest gap (2.009 eV), which indicates elevated conductivity and delocalization of charges. Different electronic modulation is observed upon adsorption: strong orbital hybridization leads to an increase in the band gap to 2.268 eV for MFM-Fe-$Sc_3P@C_{79}$, whereas the Os- and Ru-doped systems maintain low gaps (around 2.03–2.06 eV), suggesting an optimal balance between conductivity sensing and response.

1.0 Introduction

Nanotechnology has improved the design of molecular sensing systems in biomedical applications and in detecting and monitoring anticancer drugs, with the significant progress in nanotechnology [1]. Fullerenes are among the popular emerging nanomaterials that have received exceptional scientific attention because of their exceptional electronic structure, high surface area, exceptional chemical stability, and their physicochemical properties, which are tunable. Energy storage and catalysis are not the only applications of the fullerene nanostructures, and since their discovery, the range of their applications has been widened to include biosensing and drug delivery systems [2]. The fullerenes have made the spherical π-conjugated carbon structure a good candidate in the adsorption-based chemical sensors and nanoelectronic devices due to the easy delocalization of electrons [3]. Endohedral Metallofullerene (EMFs), which are products of wrapping atoms/clusters into a cage-like structure of carbon, have quite different electronic properties than pure fullerenes. The addition of metal clusters produces an internal transfer of charge between the encapsulated molecules and the carbon structure, leading to altered band structures and increased conductivity and adsorption. Density Functional Theory studies have revealed that endohedral fullerenes with a trimetallic nitride core, including $Sc_3N_8C_{80,}$ are highly charge polarized, with the internal metallic core becoming positively charged and the carbon cage negatively charged, which drastically improves intermolecular interaction and stability via adsorption [4]. The computational study of $Sc_3N@C_{80}$ adsorption systems exhibited better binding energies than the traditional C_{60} system due to the improved dispersion interaction and internal charge separation effects that stabilize adsorbate interactions and enhance sensing potential [5].

Recent reports also indicate that heteroatom doping is an effective means of improving the sensing capability of fullerenes. As an example, 60 nanostructures doped with metallic atoms (Zn and Al) have been proposed as electrochemical sensors of biomarker. Ghazwani *et al*., found doping to have a significant performance enhancement effect in sensor work. The sensor ZnC_{59}, in particular, had

remarkable characteristics: the lowest energy gap of 0.31 eV, high electrical conductance of 7.40 x 10 6 $A.m^{-2}$, high charge transfer (maximal charge transfer 28.0), and fast recovery time (2.51 x 10^{-8} s). The AlC59 was also more effective in detecting acetone, with the highest adsorptive capacity (-50.2 $kcal.mol^{-1}$) being an outstanding adsorbent. The ZnC_{59} complex had the most favorable properties with the following features: a high binding affinity to acetone that is reversible, sensitive, and can be regenerated rapidly [6]. ZnC_{59}@Ac interaction was both good and intermediate strength according to the results of QTAIM and NCI. In general, this study will confirm the usage of Zn-doped C_{60} in sensitive, reusable electrochemical sensors to detect breath acetone. Equally, theoretical studies conducted on fullerene doped network do show that the addition of heteroatoms not only disrupts carrier properties such as mobility and conductivity but also enhances electronic responsiveness necessary in nanosensor applications. The results of the research conducted by Yadav *et al* show that the 2D sheets of C_{60}, $C_{58}B_1N_1$, and $C_{54}B_3N_3$ have band gaps of about 0.97 e V (1.5 eV), 1.08 eV (1.9 eV), and 1.05 e V (1.6 eV), respectively, as calculated by PBE(HSE) [7]. Besides, as per the deformation potential theory, both doped sheets have high conductivity at high temperatures. The findings are very encouraging and highlight the importance of two individual types of BN dopants in fullerene ($C_{58}B_1N_1$) monolayers in the development of next-generation 2D nanoelectronic and photonics. In addition to sensing applications, endohedral fullerenes are also tunable to exhibit transport properties of interest in molecular electronics. Rincon-Garcia *et al* have investigated $Sc_3N@C_{80}$ cages and indicate that encapsulated cluster composition can be strategically utilized to customize transport resonances at the Fermi level and electronic responsiveness or adsorption tendencies based on molecular orientation and external perturbations [8]. Contrary to these developments, little focus has been given to phosphorus-based endohedral fullerenes and especially Sc_3PC_{80} systems. The integration of phosphorus is predicted to cause a different electronic polarization with the differences in electronegativity and bonding of phosphorus and nitrogen analogs. This replacement can have a great impact on charge transfer processes, adsorption energies, and the selectivity of sensors to pharmaceutical molecules. Further, although several computational studies have been performed to investigate fullerene interactions with gases and small biomolecules, few studies have been conducted to investigate anticancer drug sensing, in particular, metformin adsorption. Metformin, which is commonly used as an antidiabetic drug, has become of great interest in anticancer therapy in recent years. It is important to track its interaction at nanoscales, therefore, to manufacture sensitive detection platforms and drug-monitoring devices. The adsorption characteristics of metformin on engineered nanostructures offer essential data on molecular recognition, charge transfer mechanisms, and electric signal modulation, which is needed to develop sensors. This paper reports the original computational analysis of phosphorus-doped endohedral fullerene ($Sc_3P@C_{80}$) as a nanosensor to detect anticancer drugs, particularly in regard to metformin adsorption using Density Functional Theory (DFT). Contrary to the earlier research on pristine or nitrogen-based fullerenes, the phosphorus-based geometry provides a novel electronic environment, which increases charge polarization and adsorption. The study also examines transition-metal doping (Fe, Os, Ru) to systematically investigate the effects they have on charge transfer, adsorption strength, and sensing performance. Based on electronic structure calculations, NBO analysis, mapping molecular electrostatic

potential, and visualization of non-covalent interactions, the work determines the structure-property correlations in drug-surface interactions. With a specific focus on anticancer drug-sensing applications, these $Sc_3P@C_{80}$-based systems present a new generation of electronically tunable nanomaterials with higher sensitivities and better stability, extending the use of fullerene in the pharmaceutical biosensing area and providing a conceptual basis to the next generation of biomedical nanosensors.

2.0 Methodology

All quantum chemical calculations in this study were conducted within the framework of Density Functional Theory (DFT) using well-established computational tools. Molecular structures were built with GaussView 6.0.16 [9], followed by full geometry optimizations and electronic structure computations carried out using Gaussian 09 [10]. The geometries of the studied complexes were optimized at the PBE-D3/Def2-SVP level of theory [11], which provides a reliable balance between computational accuracy and efficiency, particularly for describing molecular systems and dispersion interactions. Natural Bond Orbital (NBO) analysis was performed using the NBO 3.0 module [12] integrated within Gaussian 09, enabling detailed insights into charge distribution and donor–acceptor interactions. Additional electronic and topological analyses were conducted with Multiwfn 3.8 [13], employing the Quantum Theory of Atoms in Molecules (QTAIM) framework to characterize bonding interactions. Non-Covalent Interaction (NCI) analyses were also performed, with the resulting interaction regions visualized using VMD software [14]. The chemical reactivity, electronic charge distribution, and potential biological interaction profiles of the investigated systems were further explored through Frontier Molecular Orbital (FMO) analysis, Molecular Electrostatic Potential (MESP) mapping, and the HOMO and LUMO isosurfaces were visualized using Chemcraft [15], providing a clear depiction of the electronic distributions associated with the frontier molecular orbitals.

3.0 Results and Discussion

3.1 Spin stability study

According to the computational relative energies of the various spin multiplicities of pristine and metal-doped $Sc_3P@C_{79}$ systems in Table 1, the septet spin state is apparent as the ground state of all the investigated species, with the lowest relative energy (0.00 eV) [16]. In the case of the pristine cage of $Sc_3P@C_{80}$ cage, the septet state is energetically preferred over the singlet, triplet, and quintet states by 0.21, 0.09, and 0.07 eV, respectively, pointing to a strong preference for a high-spin structure. This can be explained by the fact that various unpaired electrons are produced by the interaction of the Sc_3 cluster with the encapsulated phosphorus atom and the C_{80} carbon cage, which results in large spin polarization within the endohedral fullerene structure. The same is noted for the systems with metal doping (Fe-, Os-, and Ru-$Sc_3P@C_{79}$), with the septet state being the most stable state. In Fe-$S_{c3}P@C_{79,}$ the energy difference between the septet and singlet states is especially high (0.99 e V), which is indicative of the considerable influence of the Fe_3 d orbitals on the total magnetic moment and stabilization of the high-

spin state. The energy gaps between the singlet, triplet, and quintet states in Os- and Ru-S_3PC_{79} are relatively smaller, though the septet state is still the most energetically favored, which supports the strength of the high-spin electronic structure of the various transition metal doping. This stabilization of the septet ground-state indicates that the unpaired electron density is delocalized throughout the metal center, Sc_3P cluster, and the entire cage of the fullerene, which is likely to be key in interactions of charge transfer during the adsorption of metformin. This means that the next generation of geometry optimization and adsorption experiments is best performed on the septet spin surface, which is the real electronic ground-state structure of the M-$Sc_3P@C_{79}$ -based sensing materials.

Table 1
Relative spin stability energies (in eV) of different spin states (singlet, triplet, quintet, and septet) for pristine and transition-metal-doped $Sc_3P@C_{79}$ systems, showing the septet ground state as the most stable configuration for all cases.

M-$Sc_3P@C_{79}$	**Singlet-eV**	**Triplet-eV**	**Septet-eV**	**Quintet-eV**
$SC_3P@C_{79}$	0.21	0.09	0.00	0.07
Fe-$Sc_3P@C_{79}$	0.99	0.09	0.00	0.03
Os-$Sc_3P@C_{79}$	0.14	0.12	0.00	0.07
Ru-$Sc_3P@C_{79}$	O.14	0.12	0.00	0.07

3.2 Adsorbent Studies

The optimized bond lengths of metformin (MFM), pristine $Sc_3P@C_{80}$, transition-metal-doped $Sc_3P@C_{79}$ (Fe, Ru, and Os), and the corresponding adsorption complexes are presented in Table 2. These structural parameters provide insight into the bonding interactions, stability, and possible structural distortions occurring upon doping and adsorption. For the isolated metformin (MFM) molecule, the calculated bond lengths show typical characteristics of nitrogen-containing organic compounds. The N_4-C_3 bond length of 1.37 Å corresponds to a C-N single bond with partial double bond character due to conjugation within the guanidine group. The shorter N_5-C_3 bond (1.28 Å) suggests a stronger C = N double bond interaction. The C_{13}-H_{15} (1.10 Å) and N_{10}-H_{11} (1.01 Å) bond lengths fall within the expected range for C-H and N-H bonds, indicating stable hydrogen bonding sites within the metformin structure. In the pristine $Sc_3P@C_{80}$ system, the P_{84}-Sc_{82} bond length of 2.40 Å indicates a strong interaction between the encapsulated phosphorus atom and scandium atoms within the fullerene cage. The Sc_{83}-C_{32} bond length (2.20 Å) confirms the interaction between the scandium atom and the carbon cage, suggesting stabilization of the endohedral structure. Meanwhile, the C_{53}-C_{51} bond length of 1.45 Å corresponds to the typical C-C bond distance within fullerene frameworks, indicating that the cage retains its structural integrity. Upon transition metal doping, slight changes in bond lengths are observed. In Ru- $Sc_3P@C_{79}$, the P_{83}-Sc_{82} bond increases slightly to 2.42 Å, suggesting minor structural distortion due to the presence of the Ru

atom. The Ru_{84}-C_{16} bond length of 1.89 Å indicates strong coordination between ruthenium and the carbon atom of the fullerene surface. Similarly, in Os- $Sc_3P@C_{79}$, the Os_{84}-C_{16} bond length of 1.90 Å confirms the formation of a stable Os-C interaction. These metal-carbon interactions suggest successful surface doping of the $Sc_3P@C_{80}$ nanocluster. For the metformin adsorption complexes, additional structural changes are observed. In MFM-C_{80}, the N_{85}=C_{83} bond length of 1.89 Å and N_{89}-C_{83} bond of 1.40 Å suggest interaction between the nitrogen atoms of metformin and the fullerene surface, indicating adsorption through the nitrogen functional groups. Similarly, in MFM- $Sc_3P@C_{80}$, the N_{89}=C_{87} bond (1.28 Å) and N_{93}-C_{87} bond (1.39 Å) remain within the expected range for C = N and C–N bonds, implying that adsorption does not significantly distort the internal structure of metformin. In the metal-doped adsorption systems, stronger interactions between metformin and the doped surfaces are evident. For example, in MFM-Fe- $Sc_3P@C_{79}$, the Fe_{84}-N_{88} bond length of 2.11 Å indicates coordination between the Fe atom and the nitrogen atom of metformin, suggesting chemisorption behavior. Similarly, the Fe_{84}-C_{16} bond length of 1.81 Å confirms strong metal–carbon bonding within the modified surface. In contrast, larger metal–nitrogen distances observed in MFM-Os-$Sc_3P@C_{79}$ (Os_{84}–N_{88} = 4.11 Å) and MFM-Ru-$Sc_3P@C_{79}$ (Ru_{84}–N_{88} = 4.33 Å) indicate weaker interactions between the drug molecule and these metal centers, suggesting relatively weaker adsorption compared to the Fe-doped system. The optimized bond angles for the pristine, doped, and adsorption complexes are summarized in Table 3, revealing the geometric changes induced by metal doping and metformin adsorption. For the pristine $Sc_3P@C_{80}$ system, the Sc_{81}-P_{84}-Sc_{82} bond angle of 100.45° reflects the triangular coordination geometry formed by the scandium atoms around the encapsulated phosphorus atom. The smaller C_{30}-Sc_{83}-C_{32} angle (39.24°) indicates the curvature and constrained geometry imposed by the fullerene cage. Upon transition metal doping, notable geometric distortions occur. In Ru-$Sc_3P@C_{79}$, the Sc_{81}-P_{84}-Sc_{82} angle decreases to 41.02°, indicating structural rearrangement caused by the Ru atom. Additionally, the C_{16}-Ru_{84}-C_5 bond angle of 90.46° suggests a near-square planar coordination environment around the ruthenium center. Similar trends are observed for Os-$Sc_3P@C_{79}$, where the C_{16}-Os_{84}-C_5 angle of 90.85° indicates stable metal coordination on the fullerene surface. For the metformin molecule adsorbed on C_{80}, the N_{89}-C_{83}=N_{85} angle of 115.94° and C_{97}-N_{84}-C_{93} angle of 116.80° are consistent with the trigonal planar geometry expected around sp^2-hybridized carbon and nitrogen atoms in the metformin structure. The H_{82}-N_{89}-C_{83} angle of 108.90° reflects the typical geometry of amine groups. After adsorption onto $Sc_3P@C_{80}$, slight changes in the internal geometry of metformin occur. For example, the N_{89}=C_{87}-N_{93} angle increases to 126.20°, indicating electron redistribution due to interaction with the nanocluster surface. Additionally, the Sc_{81}-P_{84}-Sc_{82} angle remains close to its pristine value (100.21°), suggesting that the core structure of the Sc_3P cluster remains largely intact during adsorption. For the metal-doped adsorption complexes, more pronounced distortions are observed. In MFM-Fe-$Sc_3P@C_{79}$, the C_{16}-Fe_{84}-C_5 bond angle of 95.94° indicates a slightly distorted coordination geometry around the Fe atom due to the interaction with metformin. Changes in angles such as N_{89}=C_{87}-N_{93} (120.57°) further confirm the involvement of the nitrogen atoms of metformin in adsorption interactions. Similar structural variations are observed in MFM-Os-$Sc_3P@C_{79}$ and MFM-Ru-$Sc_3P@C_{79}$, where bond angles around the metal

centers and nitrogen atoms of metformin adjust to accommodate adsorption. These variations indicate that metal doping influences the adsorption orientation and interaction strength between metformin and the $Sc_3P@C_{80}$ surface.

Table 2
Selected bond lengths (Å) for studied systems

Systems	Bond labels	Bond Length-Å
MFM	N_4-C_3	1.37
	N_5-C_3	1.28
	C_{13}-H_{15}	1.10
	N_{10}-H_{11}	1.01
$Sc_3P@C_{80}$	P_{84}-Sc_{82}	2.40
	Sc_{83}-C_{32}	2.20
	C_{53}-C_{51}	1.45
Ru-$Sc_3P@C_{79}$	P_{83}-Sc_{82}	2.42
	Sc_{82}-C_{32}	2.20
	C_{50}-C_{51}	1.47
	Ru_{84}-C_{16}	1.89
Os-$Sc_3P@C_{79}$	P_{83}-Sc_{82}	2.42
	Sc_{82}-C_{32}	2.20
	C_{50}-C_{51}	1.47
	Os_{84}-C_{16}	1.90
MFM-C_{80}	C_{51}-C_{53}	1.45
	N_{85}=C_{83}	1.89
	N_{89}-C_{83}	1.40
MFM-$Sc_3P@C_{79}$	P_{84}-Sc_{82}	2.40
	Sc_{82}-C_{51}	2.20
	C_{51}-C_{52}	1.48
	N_{89}=C_{87}	1.28
	N_{93}-C_{87}	1.39

Systems	Bond labels	Bond Length-Å
MFM-Fe-$Sc_3P@C_{79}$	P_{83}-Sc_{82}	2.42
	Sc_{82}-C_{31}	2.20
	C_{50}-C_{51}	1.47
	Fe_{84}-C_{16}	1.81
	$N_{89=}C_{87}$	1.25
	Fe_{84}-N_{88}	2.11
	N_{93}-C_{87}	1.43
MFM-Os-$Sc_3P@C_{79}$	P_{83}-Sc_{82}	2.42
	Sc_{82}-C_{31}	2.20
	C_{50}-C_{51}	1.47
	Os_{84}-C_{16}	1.92
	$N_{89=}C_{87}$	1.30
	Os_{84}-N_{88}	4.11
	N_{93}-C_{87}	1.42
MFM-Ru-$Sc_3P@C_{79}$	P_{83}-Sc_{82}	2.42
	Sc_{82}-C_{31}	2.20
	C_{50}-C_{51}	1.47
	Ru_{84}-C_{16}	1.93
	$N_{89=}C_{87}$	1.29
	Ru_{84}-N_{88}	4.33
	N_{93}-C_{87}	1.39

Table 3
Selected bond angles (in degrees) for pristine, transition-metal-doped, and metformin-adsorbed $Sc_3P@C_{80}$ systems

Systems	Bond labels	Bond Angles (°)
$Sc_3P@C_{80}$	Sc_{81}-P_{84}-Sc_{82}	100.45
	C_{30}-Sc_{83}-C_{32}	39.24
Ru-$Sc_3P@C_{79}$	Sc_{81}-P_{84}-Sc_{82}	41.02
	C_{69}-Sc_{80}-C_{68}	70.42
	C_{16}-Ru_{84}-C_5	90.46
Os-$Sc_3P@C_{79}$	Sc_{81}-P_{84}-Sc_{82}	41.04
	C_{69}-Sc_{80}-C_{68}	70.47
	C_{16}-Os_{84}-C_5	90.85
Fe-$Sc_3P@C_{79}$	Sc_{81}-P_{84}-Sc_{82}	98.12
	C_{69}-Sc_{80}-C_{68}	70.45
	C_{16}-Os_{84}-C_5	93.83
MFM-C_{80}	N_{89}-C_{83}=N_{85}	115.94
	C_{97}-N_{84}-C_{93}	116.80
	H_{82}-N_{89}-C_{83}	108.90
MFM-$Sc_3P@C_{79}$	Sc_{81}-P_{84}-Sc_{82}	100.21
	C_{69}-Sc_{81}-C70	70.21
	N_{89}=C_{87}-N_{93}	126.20
	C_{97}-N_{88}-C_{101}	115.97
	H_{86}-N_{93}-C_{85}	114.21
MFM-Fe-$Sc_3P@C_{79}$	Sc_{81}-P_{84}-Sc_{82}	97.51
	C_{69}-Sc_{80}-C_{68}	39.14
	C_{16}-Fe_{84}-C_5	95.94

Systems	Bond labels	Bond Angles (º)
	N_{89}=C_{87}-N_{93}	120.57
	C_{97}-N_{88}-C_{101}	11.85
	H_{86}-N_{93}-C_{85}	11.01
MFM-Os-$Sc_3P@C_{79}$	Sc_{81}-P_{84}-Sc_{82}	97.53
	C_{69}-Sc_{80}-C_{68}	39.14
	C_{16}-Fe_{84}-C_5	88.73
	N_{89}=C_{87}-N_{93}	111.79
	C_{97}-N_{88}-C_{101}	117.05
	H_{86}-N_{93}-C_{85}	116.59
MFM-Ru-$Sc_3P@C_{79}$	Sc_{81}-P_{84}-Sc_{82}	97.94
	C_{69}-Sc_{80}-C_{68}	70.25
	C_{16}-Fe_{84}-C_5	88.55
	N_{89}=C_{87}-N_{93}	121.00
	C_{97}-N_{88}-C_{101}	116.49
	H_{86}-N_{93}-C_{85}	114.23

3.3. Non-covalent interaction (NCI) Analysis

The Non-Covalent Interaction (NCI) plots, as seen in Fig. 2, show a visualization of weak intermolecular forces in real-space, which determine the stabilization of the MFM when incubated with pristine and metal-encapsulated fullerene systems (MFM-C_{80}, MFM-$Sc_3P@C_{79}$, MFM–Fe $Sc_3P@C_{79}$, MFM–Os-$Sc_3P@C_{79}$, and MFM–Ru-$Sc_3P@C_{79}$) [20]. NCI analysis is obtained based on reduced density gradient (RDG), which determines spatial areas of low electron density and low-density gradients where non-covalent interactions are predominant [21]. They are areas of weak intermolecular forces instead of covalent bonding and are usually depicted by colored isosurfaces overlaid on $(\lambda_2)\rho$ values, where negative values represent attractions and positive values represent repulsions [22]. The blue areas indicate strong attractive forces; green areas indicate weak dispersive (van der Waals) forces and red areas indicate steric repulsive forces due to the overlap of electron density [23]. The fact that the extended green isosurfaces that exist between MFM and fullerene cage are prevailing in the MFM-C_{80} system implies that the π- π van der Waals interactions that dominate the adsorption process are mostly

dispersion driven. Such conduct is congruent with the recent theoretical examinations which have indicated that complete assemblies depending on fullerene frameworks are generally stabilized by weak dispersive forces since of the delocalized π-electron cloud of the carbon cage. This indicates that the physisorption and not chemisorption is confirmed by the absence of any substantial blue regions indicating the minimal contribution of the electrostatic or hydrogen-bonds. The same was observed in nanographene-molecule complexes where the NCI analysis showed that weak green RDG surfaces predominate host-guest stabilized in π-conjugated nanostructures. When Sc_3P is encased by C_{80}, the topology of interactions is observed to change. Appearing blue-green localized regions close to the adsorption interface are evidence of tighter attractive force between charges redistributed by the endohedral cluster. Recent studies on RDG highlight that the polarization effects, as expressed as such shifts, are electron density transfer, which changes electrostatic aspects of non-covalent bonding [24]. Relative to pristine C_{80}, the $Sc_3P@C_{80}$ complex exhibits more favorable density of interaction suggesting a greater MFM-cage affinity and higher stabilization energy. This is in line with current NCI-RDG studies which indicate that the magnitude of electrostatic contributions increases due to perturbation of molecular frameworks by metal centers on the electronic environment. A more pronounced change is realized in case of transition-metal-doped systems (Fe, Os, and Ru). The blue spots on the contact region in the Fe-$S_3P@C_{79}$ and Os-$S_3P@C_{79}$ complexes are more intense due to the existence of stronger attractive interactions between the MFM heteroatoms and the metallofullerene surface, which may be attributed to polarization of the MFM by the metal and partial charge transfer between the MFM heteroatoms and the metallofullerene surface. The modern NCI studies of transition-metal complexes are also in agreement with this fact, whereby as the metal is further incorporated, there are localized regions of attractive density, because of orbital interactions and improved electrostatic stabilization. The coexistence of red isosurfaces around delimited regions of the cage indicates steric crowding due to the extent of incorporation of metals, which signifies the strains in the structure - a phenomenon that is mostly commonly illustrated by metal-coordinated systems in which reduced interatomic distances produce repulsive RDG signatures. Among the investigated systems, it can be estimated that MFM-Ru-$Sc_3P@C_{79}$ is the most interactive system, and its surfaces are sufficiently continuous to indicate the greatest non-covalent stabilization. This behavior is consistent with more recent theoretical studies that show how heavier transition metals can both increase dispersion and polarization, and result in cooperative non-covalent stabilization in functional materials. The attractive (blue/green) vs. repulsive (red) regions demonstrate a balance of the interaction regime with a stabilization due to the dispersion forces, accompanied by the contribution of the electrostatic forces, and no longer a pure covalent bonding. Therefore, the computational results are confirmed by the comparative NCI analysis, which confirms that the incorporation of metal gradually increases the binding of compounds to metalfiller, which supports the interpretation that the transition-metal doping has a significant improvement effect on the intermolecular stabilization by modulating the electron density distribution and non-covalent interaction networks.

3.3.1 Quantum Theory of Atoms in Molecules (QTAIM)

The Quantum Theory of Atoms in Molecules (QTAIM) analysis to explain the nature, strength, and electronic nature of the interactions between Metformin (MFM) and the pristine as well as metal-doped $Sc_3P@C_{79}$ surfaces [25]. Through the analysis of the topological parameters at bond critical points (BCPs), the electron density ρ(r), Laplacian $\nabla^2\rho(r)$, energy density components, and ellipticity, in the examined systems, a definite line is drawn between weak physisorption and strong chemisorption regimes. In the MFM-$Sc_3P@C_{80}$ system, the observed BCPs of N_{91}-C_{26} and C_5-H_{104} interactions have large values of the electron density (= 0.005–0.007 a.u.) with low positive values of Laplacian (= 0.016–0.023 a.u.). The positive $\nabla^2\rho(r)$ together with near-zero and slightly positive total energy density H(r), gives evidence of closed-shell, noncovalent interactions, either of weak van der Waals forces or hydrogen bonding. Moreover, the G(r)/V(r) ratios near such close values as one and the low ELF values (< 0.025) once again prove the prevailing role of the electrostatic interactions with the insignificant orbital overlaps. These results indicate physisorption is the dominant force affecting Metformin adsorption on pristine Sc_3PC_{80} and contributes to fast sensor recovery, but at the cost of limiting sensitivity because of low charge transfer [26]. The introduction of transition metal doping on the other hand changes the interaction landscape dramatically. Fe_{84}-N_{93} form in the MFM-Fe-$Sc_3P@C_{79}$ system, is confirmed by significantly higher electron densities at the BCPs (= 0.053–0.074 a.u.) and significantly positive Laplacians (= 0.239–0.288 a.u.). Notably, H(r) develops a negative value (-0.006 -0.0007 a.u.), which signifies partial covalence. The values of G(r)/ V(r) less than one, and high ELF (to 0.190) indicate a modification and amplified exchange of electrons between the Metformin and the Fe-doped surface. It is a very desirable regime of mixed closed-shell-covalent interaction that allows very high adsorption-induced electronic perturbation without irreversible binding, which is of much interest in sensing applications. The same but stronger pattern of interaction is found in the MFM-Os-$Sc_3P@C_{80}$ system. The values of N-Os interactions are the largest of all systems of (ρ(r) 0.084 a.u., with very large values of both laplacians ($\nabla^2\rho(r)$ up to 0.324 a.u accompanied by distinctly negative H(r) values (− 0.011 to − 0.0006 a.u.). This is evidenced by these characteristics that show a more powerful chemisorptive interaction compared to Fe doping. The higher values of ELF and the ratios of λ_1/λ_3 also point out that there is directional bonding with high orbital polarization. This high-level of electronic contact suggests that there is a considerable redistribution of charges whenever Metformin is adsorbed, and this is likely to result in an intense sensor response by altering the electronic structure. In the case of the MFM-Ru-$Sc_3P@C_{79}$ system, the Ru-N interactions also have high values of electron density (0.066–0.068 a.u.) and positive values of Laplacians (0.287–0.289 a.u.), and slightly negative to near-zero values of H(r). These properties indicate moderately strong chemisorption of a partial covalent nature between the Fe- and Os-doped systems. Consistent negative ratios of λ_1/λ reflect anisotropic charge accumulation along the Ru–N bond paths, further supporting effective orbital overlap and charge transfer the results of the QTAIM clearly show that metal doping changes the weak physisorption of Metformin on $Sc_3P@C_{80}$ to a strong and chemically significant interaction, with the interaction trend. The interaction trend shows that the interaction between metal and $Sc_3P@C_{80}$ is relatively weak at the beginning of the series and becomes stronger and stronger as the electron density at the Regarding sensing, the metal-doped

systems, especially Os- and Fe-doped Sc_3PC_{79}, provide the best ratio between adsorption capabilities and electronic sensitivity to offer a solid theoretical basis of improved Metformin detection.

3.4 HOMO-LUMO analysis

The reactivity and sensing ability of the pristine and metalled Sc_3PC_{80} systems on the adsorption of Metformin were also tested using frontier molecular orbital (FMO) analysis and other global reactivity indices [27]. Direct understanding of the electronic sensitivity, charge-transfer capacity, and conductivity modulation of the proposed materials as sensor elements is provided by the HOMO and LUMO energies, band gap (Eg), chemical hardness (eta) and softness (S). In the case of pristine Sc_3P_{80}, the HOMO-LUMO gap is relatively large (2.499 eV), and the chemical hardness (0.2 eV) was high, and the softness was relatively low. This electronic rigidity shows restricted charge-transfer responsiveness, which is in line with weak physisorptive interaction with Metformin as determined by the QTAIM analysis. When the pristine cage (MFM-$Sc_3P@C_{79}$) is adsorbed by Metformin, it is indicated by a slight decrease in the band gap (2.470 eV) and insignificant alterations in the hardness and softness. This confirms that Metformin only causes slight changes in the electronic structure of undoped $Sc_3P@C_{80}$, thus reducing its sensing performance in the absence of surface modification. Conversely, metal doping helps to increase the intrinsic reactivity of $Sc_3P@C_{80}$ greatly. The Fe-, Os-, and Ru-doped systems have much smaller band gaps (2.012.08 eV) than the pristine cage, which is due to a higher degree of electronic delocalization and conductivity. The lowest band gap (2.009 eV) and hardness (approximately 1.00 eV) were found in Os-$Sc_3P@C_{80}$, which is the most reactive intrinsically and most able to accept the electron before adsorption. The trend indicates the usefulness of transition-metal doping to activate the fullerene surface to be used in sensing. When Metformin is adsorbed, significant electronic modulation can be noticed in all metal-doped systems, which is evidence of a strong sensor-analyte coupling. In the case of MFM-Fe-$Sc_3P@C_{79}$, the band gap rises to 2.268 eV with an increment in the hardness and a decrease in the softness. This increase in bandgap indicates charge redistribution and orbital rehybridization caused by Fe-N bonding, which agrees with the mixed covalent interaction as indicated by QTAIM. Even though the rise in Eg can in some ways lower conductivity, the extent of change constitutes a measurable electronic signal that can be used in chemi-resistive sensing. The MFM-Os-Sc_3PC_{79} and MFM-Ru-$Sc_3P@C_{79}$ systems have better sensing properties. Bands following adsorption (around 2.032.06 eV) in both cases are near the adsorption values, but there is a strong upward displacement of HOMO and LUMO levels. The changes indicate high charge transfer between Metformin and the metal-doped fullerene surface, which causes high-intensity Fermi-level modification. This low hardness and high softness left after adsorption suggest that the electronic flexibility is maintained, and the required sensor sensitivity and fast signal transduction. Compared to it, the reactivity analysis shows a definite rank of sensing performance. Indeed, Pristine Sc_3PC_{80} demonstrates insignificant electronic response to Metformin, but on the one hand, the metallic doping increases the chemo-responsiveness and sensitivity significantly [28]. The doped systems, Os- and Ru-doped $Sc_3P@C_{79}$, are a good balance between high adsorption-induced electronic perturbation and retain conductivity, whereas Fe doping has a stronger yet less flexible interaction.

Table 4
Calculated frontier molecular orbital energies and global reactivity descriptors for $Sc_3P@C_{80}$-based adsorbents before and after Metformin adsorption.

Systems	E_{HOMO}-eV	E_{LUMO}-eV	Eg-eV	σ-eV^{-1}	□-eV
Fe-$Sc_3P@C_{79}$	-5.650	-3.567	2.082	1.041	0.521
Os-$Sc_3P@C_{79}$	-5.457	-3.447	2.010	1.005	0.502
Ru-$Sc_3P@C_{79}$	-5.546	-3.501	2.045	1.022	0.511
$Sc_3P@C_{80}$	-5.940	-3.441	2.499	1.250	0.625
Fe-$Sc_3P@C_{79}$	-5.649	-3.567	2.082	1.041	0.521
MFM-C_{80}	-5.7171	-4.7383	0.979	2.348	0.149
MFM-Fe-$Sc_3P@C_{79}$	-5.416	-3.147	2.268	1.134	0.567
MFM-Os-$Sc_3P@C_{79}$	-4.912	-2.853	2.059	1.030	0.515
MFM-Ru-$Sc_3P@C_{79}$	-4.754	-2.720	2.034	1.017	0.508
MFM-$Sc_3P@C_{79}$	-5.912	-3.442	2.470	1.235	0.618

3.4.1 Density of State (DOS) analysis

The density of states (DOS) spectra present a finer image of the effect on the electronic structure of $Sc_3P@C_{80}$ by metal doping and, by extension, its sensing power. Using the comparison of the DOS profiles of pristine and metal-doped systems, it becomes evident that there is increased electronic activity near the Fermi level, which is one of the main requirements of chemiresistive sensing [29]. In the case of pure ScP_3C_{80}, the width of the forbidden gap in the DOS spectrum is relatively large at the Fermi level, and the band gap is about 2.50 eV. The occupied states confined to the virtual states are far apart, which implies scarce availability of charge carriers on the ambient conditions. This computer feature justifies the relatively low intrinsic conductivity and the poor sensing reaction of the undoped system, which correlates with the HOMO-LUMO examination and a physisorptive connection found in QTAIM. When the metal is doped, it is found that there is a strong alteration of the DOS distribution. In the Fe-$Sc_3P@C_{79}$ system, the DOS at the Fermi level is significantly larger, and the band gap is reduced to approximately 2.08 e V. The formation of new electronic states in the immediate surroundings of the Fermi level can be explained by the hybridization of Fe d-orbitals with the π-systems of the fullerene cage. This hybridization increases the charge delocalization and allows the transfer of electrons and thus increases the baseline conductivity of sensor material. An analogous but somewhat more intense effect is also present in the Os-$Sc_3P@C_{79}$ system, which shows the best band gap of any of the doped structures (≈ 2.01 eV), which suggests that there are more orbital overlap and better electronic

interaction. This finding is completely in line with the QTAIM finding, which had found stronger Os interactions in the presence of N and implies that in sensing applications, Os doping is specifically suitable to activate Sc_3PC_{80}. Ru-$Sc_3P@C_{79}$ system has an intermediate nature, as the band gap is about 2.03–2.05 eV and DOS intensity has a significant enhancement around the Fermi level as compared to pristine $Sc_3P@C_{80}$. The features of the DOS suggest moderate yet vast hybridization of Ru d-states with the entire fullerene orbitals resulting in improved electronic responsiveness without loss of structural integrity. This electronic alteration is symmetrical with the HOMO-LUMO and reactivity parameters which showed that the Ru-doped system had good softness and moderate hardness. Its comparative analysis reveals that DOS analysis verifies that transition metal doping causes new electronic states and alters occupied and virtual orbitals to the Fermi level to reduce the band gap and increase electrical conductivity. Together with the QTAIM and HOMO-LUMO analysis, the DOS outcome demonstrates solid theoretical data showing that metal-doped $Sc_3P@C_{79}$ is a highly efficient candidate in the detection of Metformin in a sensitive and reliable way, especially with the Os- and Ru-doped systems.

3.4.2 Molecular Electrostatic potential (MESP) Analysis

The molecular electrostatic potential (MESP) surfaces of metformin (MFM) adsorbed on pristine and transition-metal-functionalized $Sc_3P@C_{80}$ nanostructures are presented in Fig. 4. MESP analysis provides important insight into the charge distribution, electrophilic and nucleophilic reactive regions, and possible interaction sites between the adsorbent nanostructures and the metformin molecule. In the MESP maps, the electrostatic potential is represented by a color scale ranging from negative potential (red) to positive potential (blue), while green regions represent nearly neutral electrostatic potential. Negative regions correspond to electron-rich sites favorable for electrophilic attack, whereas positive regions indicate electron-deficient sites susceptible to nucleophilic interactions. For the MFM-C_{80} complex, the MESP surface shows a clear charge separation between the metformin molecule and the fullerene cage. The red regions localized around the nitrogen atoms of metformin indicate high electron density arising from lone pair electrons on the nitrogen atoms, which serve as potential adsorption sites for interaction with the nanostructure. Meanwhile, the surface of the C_{80} fullerene cage predominantly exhibits green to light blue regions, suggesting relatively neutral to slightly positive electrostatic potential. This distribution indicates that the adsorption interaction is mainly driven by electrostatic attraction between the electron-rich nitrogen atoms of metformin and the electron-deficient regions of the fullerene surface.

In the case of the MFM–$Sc_3P@C_{79}$ system, the MESP surface demonstrates a noticeable redistribution of charge due to the presence of the encapsulated Sc_3P cluster. The interior phosphorus–scandium unit induces localized polarization within the carbon cage, which modifies the electrostatic potential on the surface of the fullerene. The metformin molecule still shows intense negative potential around the nitrogen atoms, while the region of the fullerene closest to the adsorbed molecule exhibits slightly positive potential, indicating enhanced electrostatic attraction and stabilization of the adsorption complex.

For the transition-metal-functionalized systems (Fe, Os, and Ru), the MESP surfaces reveal more pronounced charge redistribution due to the presence of the metal atoms. In the MFM–Fe-$Sc_3P@C_{79}$ complex, the electrostatic potential around the Fe atom shows significant polarization, producing regions of positive potential that facilitate stronger interaction with the electron-rich nitrogen atoms of metformin. This interaction results in noticeable charge transfer between the drug molecule and the functionalized nanostructure, which is reflected in the stronger adsorption behavior observed for the Fe-decorated system.

Similarly, the MFM-Os-$Sc_3P@C_{79}$ and MFM-Ru-$Sc_3P@C_{79}$ complexes show modifications in the electrostatic potential distribution around the metal centers. The presence of Os and Ru introduces localized positive potential regions on the nanocluster surface, which serve as favorable adsorption sites for the negatively charged regions of metformin. However, compared to the Fe-functionalized system, the charge polarization appears slightly less pronounced, suggesting relatively weaker electrostatic interactions with the drug molecule. The MESP analysis indicates that the nitrogen atoms of metformin are the primary reactive sites involved in adsorption, while the metal-functionalized $Sc_3P@C_{80}$ nanostructures provide favorable electrostatic environments that enhance the interaction strength. The observed charge redistribution and polarization effects confirm that transition-metal decoration improves the sensing capability of the $Sc_3P@C_{80}$ nanocluster toward metformin detection. These findings are consistent with the adsorption energy results and further support the suitability of metal-doped $Sc_3P@C_{80}$ nanostructures as potential nanosensors for anticancer drug monitoring.

3.5 NBO Analysis

According to the NBO charge transfer analysis, the nature and strength of the interactions between metformin (MFM) and pristine or metal-doped $Sc_3P@C_{80}$ system can be well explained in terms of donor- acceptor interactions and other stabilization energies of the second order, $E^{(2)}$. In the case of the MFM-C_{80} system, π→σ* and σ→π* charge transfers between the fullerene cage functional groups and metformin functional groups are relatively weak with low values of $E^{(2)}$ (0.07–0.26 kcal/mol). Such low stabilization energies, along with small F(i,j) values, are indicative of weak physisorption dominated by dispersion and small orbital overlap, which is expected of minimal electronic communication of metformin and the pristine C_{80} surface [32]. When the Sc_3P cluster and the transition metal doping is incorporated, the charge transfer interactions have been observed to be more intense. In MFM-Fe-$Sc_3P@C_{80}$ system, $\sigma C_{85}–N_{91} \rightarrow LP^*(3)Fe_{84}$ by direct electron donation of metformin to the Fe center is observed ($E^{(2)}$ 0.30 kcal/mol). Other π→σ* and σ→π* reactions between the Sc-P unit and the metformin backbone also prove the increased orbital mixing enabled by the metal core. This is more interaction of the donor and the acceptor indicating that Fe doping successfully exposes the fullerene surface in more energetic association with the metformin. In MFM-Os-$Sc_3P@C_{79}$, the highest charge transfer interaction is found, in particular, the $\sigma C_{18}–Os_{84} \rightarrow \sigma^*C_{85}–N_{91}$ donation with a high $E_{(2)}$ value of 2.35 kcal/mol and a large F(i,j) value (0.034 a.u).Such a large stabilization energy shows a high level of orbital overlap and

good two-way charge transfer between metformin and the Os-doped $Sc_3P@C_{80}$ cage. The existence of the complementary back-donation interactions also testifies to the development of strong adsorption complex, which in turn means that Os doping significantly increases the sensing performance due to the strong electronic interactions. Equally, MFM–Ru–Sc3P@C_{80} system displays considerable charge transfer, specifically, the $\sigma C8_5–N_{91} \rightarrow LP^*(3)\ Ru_{84}$ with an $E^{(2)}$ of 1.16 kcal/mol. The presence of Ru lone pair antibonding orbitals is an indicator of successful electron donation of the metformin to the Ru center, with other σ-σ interactions contributing to the stability of adsorption. These findings indicate that the process of Ru doping is also conducive to the stronger chemisorption than in the pristine system, but weaker than the Os-doped analogue. Conversely, the MFM-$Sc_3P@C_{80}$ system, in which the metformin molecules are not externally doped with metal, reveals comparatively weak 0 - interactions, and $E^{(2)}$ values are low (0.05–0.11 kcal/mol), which means that the cage does not delocalize charges on the metformin molecules. In general, the NBO analysis indicates that the possession of transition metal doping, especially those of Os and Ru, is very helpful in increasing the charge transfer of both metformin and $Sc_3P@C_{80}$, therefore, enhancing adsorption and electronic sensitivity of these systems. This interaction between the donor and the acceptor promotes the efficient sensing activity of M-$Sc_3P@C_{79}$ to metformin detection.

3.5.1 NBO population analysis

The Natural Bond Orbital (NBO) analysis of populations gives a close insight into the redistribution of electrons between the MFM and the complete fullerene-based systems, and by quantifying the atomic charges and electrostatic transfer of charge [33]. NBO charges can be used to determine the localization of electron density on atoms following bonding interactions and to determine how metal encapsulation can affect electronic structure (i.e., donor/acceptor behavior). Based on your findings, the values of the total charges evidently show progressive charge transfer MFM compound to the metallofullerene skeleton as more metal is incorporated with the magnitude being as follows: $Q_{MFM-Fe-Sc3P@C79}$ (0.551) > $Q_{MFM-Os-Sc3P@C79}$ (0.335) > $Q_{MFM-Ru-Sc3P@C79}$ (0.292) > $Q_{MFM-Sc3P@C79}$ (0.276) The existence of the neutral charge in MFM-C_{80} indicates no electron transfer, and positive total charges in metallofullerene systems indicate the transfer of electrons from the compound to the cage in response to the polarization of the metal-cluster in these systems. The comparison of carbon atoms in more detail reveals that positive charge within Fe-containing systems is raised (e.g., C: 0.629 → 0.695 and 0.639 → 0.715) which depicts the withdrawal of electrons in the MFM carbons and their density. This rise is due to high electron-accepting properties of the Fe-$Sc_3P@C_{80}$ cage that boosts MFM-to-cage charge transfer caused by orbital overlap and electrostatic attraction. On the contrary, Os and Ru systems have lower positive charges of carbon (as 0.609 − 0.563 and 0.531 − 0.522 ranges), which suggests partial back-donation of heavy metals. Diffuse d-orbitals of Os and Ru permit more redistribution of the electron density towards the MFM reducing the carbon electron depletion relative to Fe. The nitrogen atoms as the primary donors of electrons because of the lone pairs have significant changes in charge which are direct representation of the strength of co-ordination. Some of the nitrogen atoms in the Fe complex become less negative

(e.g. -0.687 -0.739 or -0.650 -0.732) which is a sign of increased electron donation to the metallofullerene and the strength of the donor acceptor interaction. This decrement of the electron density is due to the fact that Fe is comparatively more electronegative in interaction with other electrons in the cluster and charge is withdrawn. Os and Ru systems, in contrast, exhibit relatively smaller changes (− 0.616 to -0.589 range), which indicates more equal sharing of electrons than intensive extracting of electrons. Only the $Sc_3P@C_{80}$ system behaves intermediately, which validates that the cage polarization of encapsulated metals occurs in the absence of exogenous transition-metal substitution. The hydrogen atoms always become a little more positive throughout metallofullerene complex (e.g., 0.357 0.417 or 0.374 0.424 in Fe systems) [34]. This effect is indirectly caused by electron density loss to nearby nitrogen and carbon atoms; the closer the electron density moves to the cage, the weaker the shielding of the bonded hydrogens, which increases positive NBO charges. Its effect is greatest in Fe complexes and least in pristine C_{80}, again supporting the observation of increasing polarization with increasing metal incorporation. This general charge redistribution process can be explained, in turn, by three key electronically determined reasons which are: metal-induced polarization, in which encapsulated Sc_3P distorts the electron density of the entire cage of fullerene; MFM-to-cage charge transfer, most effectively with Fe because of the effective overlap of orbital with the strongest polarizable d-orbital; and metal back-donation, more pronounced in the Os and Ru systems because of larger and more polarizable d-orbital in the heavier transition metals and more even distribution These electronic consequences account for why Fe systems are the most active with the total charge transfer, whilst Os and Ru complexes are moderated but stabilized to reorganize electrons. Comparatively, the NBO analysis confirms that Fe replacement facilitates the greatest electron withdrawal and highest donor-acceptor contact whereas Os and Ru inject electronic delocalization and balanced charge stabilization and $Sc_3P@C_{80}$ encapsulation by itself offers average polarization contrasting pristine C_{80}. The charge differences you see clearly support your results on MESP and NCI in which stronger regions of electrostatic complementarity and interaction are observed within the metal-containing systems, and this indicates that tightening of binding is a result of metal-induced charge transfer and redistribution in the MFM-metallofullerene mutualities.

3.6 Adsorption studies: Charge on metal, BSSE, and Solvation energies

As indicated by the adsorption and solvation parameters in **Table 8**, the strength of the interaction, the nature of charge transfer, and the stability of metformin (MFM) on pristine and metal-doped $ScP@C_{80}$ systems can be readily understood. The adsorption energy (E_{ads}) is one of the key metrics of the binding strength with lower values of the adsorption energy reflecting the potential strength of adsorption [35]. With a relatively small adsorption energy of -0.54 eV -0.53 eV (after-BSSE) in the pristine MFM-C_{80} system, one would conclude that it is weak physisorption, that is dominated by van der Waals forces without any significant charge transfer. The absence of a net charge transfer (Q_M) and small solvation stabilization ($\Delta E_{solvation}$- 0.36 eV) are also indicative of a weak interaction [36] that implies that pristine C_{80} is not very sensitive to metformin detection. Conversely, the metal doping increases the adsorption

of metformin on the $Sc_3P@C_{80}$ framework to a great extent. The complex of MFM-FeSc_3PC_{79} has a significantly lower adsorption energy (-2.18 e V, made negative by adjusting the complex position), with a quantifiable charge transfer of 0.10 e between the metformin and the substrate. This high rise in adsorption strength is an indication of the intensive chemisorptive interactions that are produced through Fe center which is an effective electron acceptor. The high solvation energy (– 1.30 eV) also points to the fact that the Fe-doped system is held in an excited state under solvated conditions, yet another essential requirement regarding the practical use in sensing of biological environments. The interaction is even stronger between the MFM-Os- $Sc_3P@C_{79}$ system, where the adsorption energies are – 2.67 eV (-2.66 eV after BSSE) and the charge transfer of 0.07 e. This increased adsorption has been explained by the high participation of d-orbital of Os to facilitate good orbital overlap and charge delocalization at the site of adsorption. This is supported by the lower solvation energy (-1.46 eV), which suggests that the adsorption complex is more stable in solvent effects. The MFM-Ru-$Sc_3P@C_{79}$ complex has the most pronounced interaction with metformin, with the most negative adsorption energy (-2.91 eV -2.90 eV with BSSE correction) and charge transfer value (0.13 -1 of an electron). These findings indicate a strong chemisorption due to a close electronic interaction between metformin and the Ru-doped $Sc_3P@C_{79}$ surface. The solvation energy corresponding (-1.66 eV) is also the largest in magnitude meaning it is better stabilized in aqueous or biological environment which is much desirable in sensor performance. Interestingly, the MFM system with the $Sc_3P@C_{80}$ is less strongly adsorbed (E_{ads} = -0.18 eV); the adsorption energy with bases set superposition (E_{ads} -2.17 eV) indicates that the effect of basis set superposition has a strong impact on the interaction energy in this scenario. However, the solvation energy is relatively low (i.e., -0.39 eV) and no clear transfers of charge occurred, suggesting that in comparison to transition metal-doped systems the $Sc_3P@C_{80}$ substrate alone is not particularly good in promoting metformin adsorption. The integrated adsorption energy, charge transfer, BSSE correction, and solvation analysis have conclusively shown that transition metal doping was able to significantly enhance the strength of interaction and environment stability of $Sc_3P@C_{80}$ with metformin. The adsorption activity of Ru-$_3P@C_{80}$ has the highest potential in the sensing of metformin in the highly sensitive regimes.

Table 5
Adsorption energies (E_{ads}, eV), corrected adsorption energies with basis set superposition error (E_{ads}+BSSE, eV), solvation energy corrections ($\Delta E_{solvation}$, a.u. and eV), and charge transfer (Q_M, e) for metformin adsorption on pristine and transition-metal-doped $Sc_3P@C_{80}$ systems

Systems	**E_{ad} (eV)**	Q_M	**$E_{ads+BSSE}$**	**$\Delta E_{solvation}$ e.v**
MFM-C_{80}	-0.54	-	-0.53	-0.36
MFM-Fe-$Sc_3P@C_{79}$	-2.18	0.10	-2.15	-1.30
MFM-Os-$Sc_3P@C_{79}$	-2.67	0.07	-2.66	-1.46
MFM-Ru-$Sc_3P@C_{79}$	-2.91	0.13	-2.90	-1.66
MFM-$Sc_3P@C_{79}$	-0.18	-	-2.17	-0.39

4.0 Conclusions

This paper shows that phosphorus-doped endohedral fullerenes, especially $Sc_3P@C_{80}$, are promising nano-scaffolds of sensitive pharmaceutical detection. An analysis conducted through the density-functional theory demonstrated that pristine $Sc_3P@C_{80}$ zero interacts with metformin through physisorption with minimum structural distortion and electronic response. These doping with Fe, Ru, and Os provide dramatic changes in adsorption behavior and electronic sensitivity with Fe leading to chemisorption via Fe–N bond formation and Ru/Os providing an ideal balance between adsorption strength and electronic flexibility. The band gap analysis showed that metal doping lowers energy gaps (= 2.01–2.08 eV), which contributes to better charge delocalization and conductivity and DOS, NBO, QTAIM, and NCI analyses revealed that the orbital hybridization is stronger, that the interaction of the donor and acceptor is improved, and that the ability to transfer charges in metal-doped systems are increased. Os- and Ru-doped $Sc_3P@C_{79}$ boards had the most reasonable combination of adsorption energy, electronic modulation and spin stability among the systems investigated indicating their potential application as highly responsive nanoplatforms in detecting metformin. On the whole, the present work demonstrates that transition-metal-doped $Sc_3P@C_{79}$ can be used as an electronically tunable high-performance sensor, which justifies the design of the next-generation metallofullerene-based nanosensors to biomedical and anticancer drug monitoring.

5.0 Declarations

5.1 Ethics approval and consent to participate

Not applicable

5.2 Availability of data and material

All data are contained within the manuscript and the supporting information.

5.3 Competing interests

All authors confirm that no financial or personal conflict of interest could have impacted the research work or findings presented in this research paper.

5.4 Funding

This research was not funded by any Governmental or Non-governmental agency.

5.5 Authors' Contributions

Lubem Aondoakaa: Conceptualization and Supervision. **Musa Runde**: Project Administration, Methodology and Resources. **David John**: Writing, Editing and Visualization. **Chukwuebuka E. Mgbemere**: Data Curation and Validation. **Omobolanle Rofiat Savage**: Writing, Editing and Proofreading.

References

1. Mosleh-Shirazi, S. et al. Nanotechnology advances in the detection and treatment of cancer: an overview. *Nanotheranostics* **6** (4), 400. https://doi.org/10.7150/ntno.74613 (2022).
2. Baskar, A. V. et al. Self-assembled fullerene nanostructures: synthesis and applications. *Adv. Funct. Mater.* **32** (6), 2106924. https://doi.org/10.1002/adfm.202106924 (2022).
3. Adeleye, A. P., Gulack, A. O. & Aondoakaa, L. Engineering rhodium encapsulated indium doped fullerene for NH3, NO, and NO2 sensing. *Sci. Rep.* https://doi.org/10.1038/s41598-025-93796-7 (2025).
4. Karle, N. N. *DFT Study of Adsorption of Trimetallic Endohedral Fullerenes on Graphene* (The University of Texas at El Paso, 2017).
5. Reveles, J. U., Karle, N. N., Baruah, T. & Zope, R. R. Electronic and structural properties of C60 and Sc3N@ C80 supported on graphene nanoflakes. *J. Phys. Chem. C*. **120** (45), 26083–26092. https://pubs.acs.org/doi/10.1021/acs.jpcc.6b07405 (2016).
6. Ghazwani, M. & Hani, U. High-performance electrochemical sensors based on doped C60 fullerene for non-invasive diabetes diagnosis and environmental acetone removal: a computational study. *Sci. Rep.* **15** (1), 41089. https://doi.org/10.1038/s41598-025-24911-x (2025).
7. Yadav, V. K. Bn doping in the realm of two-dimensional fullerene network for unparalleled structural, electronic, optical, and her advancements: A cutting-edge dft investigation. *arXiv preprint arXiv:2308.06723*. (2023). https://doi.org/10.48550/arXiv.2308.06723
8. Rincón-García, L., Ismael, A. K., Evangeli, C., Grace, I., Rubio-Bollinger, G., Porfyrakis,K., … Lambert, C. J. (2016). Molecular design and control of fullerene-based bi-thermoelectric materials. Nature

materials, 15(3), 289–293. https://doi.org/10.1038/nmat4487.

9. Kebiroglu, H. & Yılmaz, M. Investigation of UV-Visible absorption quantum effects doped of norepinephrine, Mg + 2 atom by using DFT method. *J. Phys. Chem. Funct. Mater.* **6** (2), 145–151. https://doi.org/10.54565/jphcfum.1332113 (2023).
10. Frisch, A. gaussian 09W Reference. *Wallingford Usa*. **470** (4), 25 (2009).
11. Li, B., Zhang, X., Stauber, J. M., Miller, I. I. I., Spokoyny, A. M. & T. F., & Electronic structure of superoxidized radical cationic dodecaborate-based clusters. *J. Phys. Chem. A*. **125** (28), 6141–6150. https://doi.org/10.1021/acs.jpca.1c03927 (2021).
12. Bağlan, M., Gören, K. & Yıldıko, Ü. HOMO–LUMO, NBO, NLO, MEP analysis and molecular docking using DFT calculations in DFPA molecule. *Int. J. Chem. Technol.* **7** (1), 38–47. https://doi.org/10.32571/ijct.1135173 (2023).
13. Fekadu, S., Hordofa, A. K., Belay, A., Sherefedin, U., Asefa, J., Thillainayaga, G.,… Mahamud, J. H. (2025). DFT-and Multiwfn-driven investigation of 1-benzofuran: Structural,topological, natural bond orbital, Hirshfeld surface, and interaction energy analyses,coupled with molecular docking of pyrazole and chalcone for anti-breast cancer exploration.AIP Advances, 15(8). https://doi.org/10.1063/5.0285742.
14. Humphrey, W., Dalke, A. & Schulten, K. VMD: visual molecular dynamics. *J. Mol. Graph.* **14** (1), 33–38. https://doi.org/10.1016/0263-7855(96)00018-5 (1996).
15. Han, J. Chemcraft: a ludic approach to educational game design. In *extended abstracts of the 2021 CHI conference on human factors in computing systems* (pp. 1–5). (2021)., May https://doi.org/10.1145/3411763.3451854
16. Chapyshev, S. V., Walton, R., Sanborn, J. A. & Lahti, P. M. Quintet and septet state systems based on pyridylnitrenes: Effects of substitution on open-shell high-spin states. *J. Am. Chem. Soc.* **122** (8), 1580–1588. https://doi.org/10.1021/ja993131c (2000).
17. Saini, R. S., Mosaddad, S. A. & Heboyan, A. Application of density functional theory for evaluating the mechanical properties and structural stability of dental implant materials. *BMC Oral Health*. **23** (1), 958. https://doi.org/10.1186/s12903-023-03691-8 (2023).
18. Li, B., Gao, W. & Jiang, Q. Electronic and geometric determinants of adsorption: fundamentals and applications. *J. Physics: Energy*. **3** (2), 022001. 10.1088/2515–7655/abd295 (2021).
19. Leininger, M. L., Van Huis, T. J. & Schaefer, H. F. Protonated high energy density materials: N4 tetrahedron and N8 octahedron. *J. Phys. Chem. A*. **101** (24), 4460–4464. https://doi.org/10.1021/jp970258k (1997).
20. Otero-De-La-Roza, A., Johnson, E. R. & Contreras-García, J. Revealing non-covalent interactions in solids: NCI plots revisited. *Phys. Chem. Chem. Phys.* **14** (35), 12165–12172. https://doi.org/10.1039/C2CP41395G (2012).
21. Saleh, G., Gatti, C., Lo Presti, L. & Contreras-García, J. Revealing non-covalent interactions in molecular crystals through their experimental electron densities. *Chemistry–A Eur. J.* **18** (48), 15523–15536. https://doi.org/10.1002/chem.201201290 (2012).

22. Lu, T. Visualization analysis of covalent and noncovalent interactions in real space. *Angew. Chem. Int. Ed.* **64** (29), e202504895. https://doi.org/10.1002/anie.202504895 (2025).
23. Lu, C., Chen, P., Li, C. & Wang, J. Study of intermolecular interaction between small molecules and carbon nanobelt: Electrostatic, exchange, dispersive and inductive forces. *Catalysts* **12** (5), 561. https://doi.org/10.3390/catal12050561 (2022).
24. Saleh, G., Gatti, C., Lo Presti, L. & Contreras-García, J. Revealing non-covalent interactions in molecular crystals through their experimental electron densities. *Chemistry–A Eur. J.* **18** (48), 15523–15536. https://doi.org/10.1002/chem.201201290 (2012).
25. Cukrowski, I., de Lange, J. H. & Mitoraj, M. Physical nature of interactions in ZnII complexes with 2, 2'-bipyridyl: Quantum theory of atoms in molecules (QTAIM), interacting quantum atoms (IQA), noncovalent interactions (NCI), and extended transition state coupled with natural orbitals for chemical valence (ETS-NOCV) comparative studies. *J. Phys. Chem. A*. **118** (3), 623–637. https://doi.org/10.1021/jp410744x (2014).
26. Aljadaani, A. H., Yakout, A. A. & Abdel-Aal, H. Enhanced Adsorption of Metformin Using Cu and ZnO Nanoparticles Anchored on Carboxylated Graphene Oxide. *Polymers* **18** (1), 71. https://doi.org/10.3390/polym18010071 (2025).
27. Arshad, M., Arshad, S., Majeed, M. K., Frueh, J., Chang, C., Bilal, I., … Yasir Mehboob,M. (2023). Transition Metal-decorated Mg12O12 nanoclusters as biosensors and efficient drug carriers for the Metformin anticancer drug. ACS omega, 8(12), 11318–11325..
28. Skinner, H. D., McCurdy, M. R., Echeverria, A. E., Lin, S. H., Welsh, J. W., O'Reilly,M. S., … Guerrero, T. M. (2013). Metformin use and improved response to therapy in esophageal adenocarcinoma. Acta Oncologica, 52(5), 1002–1009. https://doi.org/10.3109/0284186X.2012.718096.
29. Bulemo, P. M., Kim, D. H., Shin, H., Cho, H. J., Koo, W. T., Choi, S. J., … Kim, I.D. (2025). Selectivity in chemiresistive gas sensors: strategies and challenges. Chemical reviews, 125(8), 4111–4183.https://doi.org/10.1021/acs.chemrev.4c00592.
30. Lebedeva, M. A., Chamberlain, T. W. & Khlobystov, A. N. Harnessing the synergistic and complementary properties of fullerene and transition-metal compounds for nanomaterial applications. *Chem. Rev.* **115** (20), 11301–11351. https://doi.org/10.1021/acs.chemrev.5b00005 (2015).
31. Suresh, C. H. & Anila, S. Molecular electrostatic potential topology analysis of noncovalent interactions. *Acc. Chem. Res.* **56** (13), 1884–1895. https://doi.org/10.1021/acs.accounts.3c00193 (2023).
32. Aljadaani, A. H., Yakout, A. A. & Abdel-Aal, H. Enhanced Adsorption of Metformin Using Cu and ZnO Nanoparticles Anchored on Carboxylated Graphene Oxide. *Polymers* **18** (1), 71. https://doi.org/10.3390/polym18010071 (2025).
33. Xu, F. *Theoretical Study of Electron Transport Properties of Fullerene-based Low-dimensional Nanoelectronic Devices* (Doctoral dissertation). (2015). https://hdl.handle.net/1911/87792

34. Sarfaraz, S., Yar, M. & Ayub, K. The electronic properties, stability and catalytic activity of metallofullerene (M@ C60) for robust hydrogen evolution reaction: DFT insights. *Int. J. Hydrog. Energy*. **51**, 206–221. https://doi.org/10.1016/j.ijhydene.2023.08.123 (2024).
35. Gao, W. et al. Determining the adsorption energies of small molecules with the intrinsic properties of adsorbates and substrates. *Nat. Commun.* **11** (1), 1196. https://doi.org/10.1038/s41467-020-14969-8 (2020).
36. Kumar, S. & Panja, S. K. Intermolecular charge-transfer complex between solute and ionic liquid: experimental and theoretical studies. *Theor. Chem. Acc.* **142** (12), 126. https://doi.org/10.1007/s00214-023-03073-x (2023).

Figures

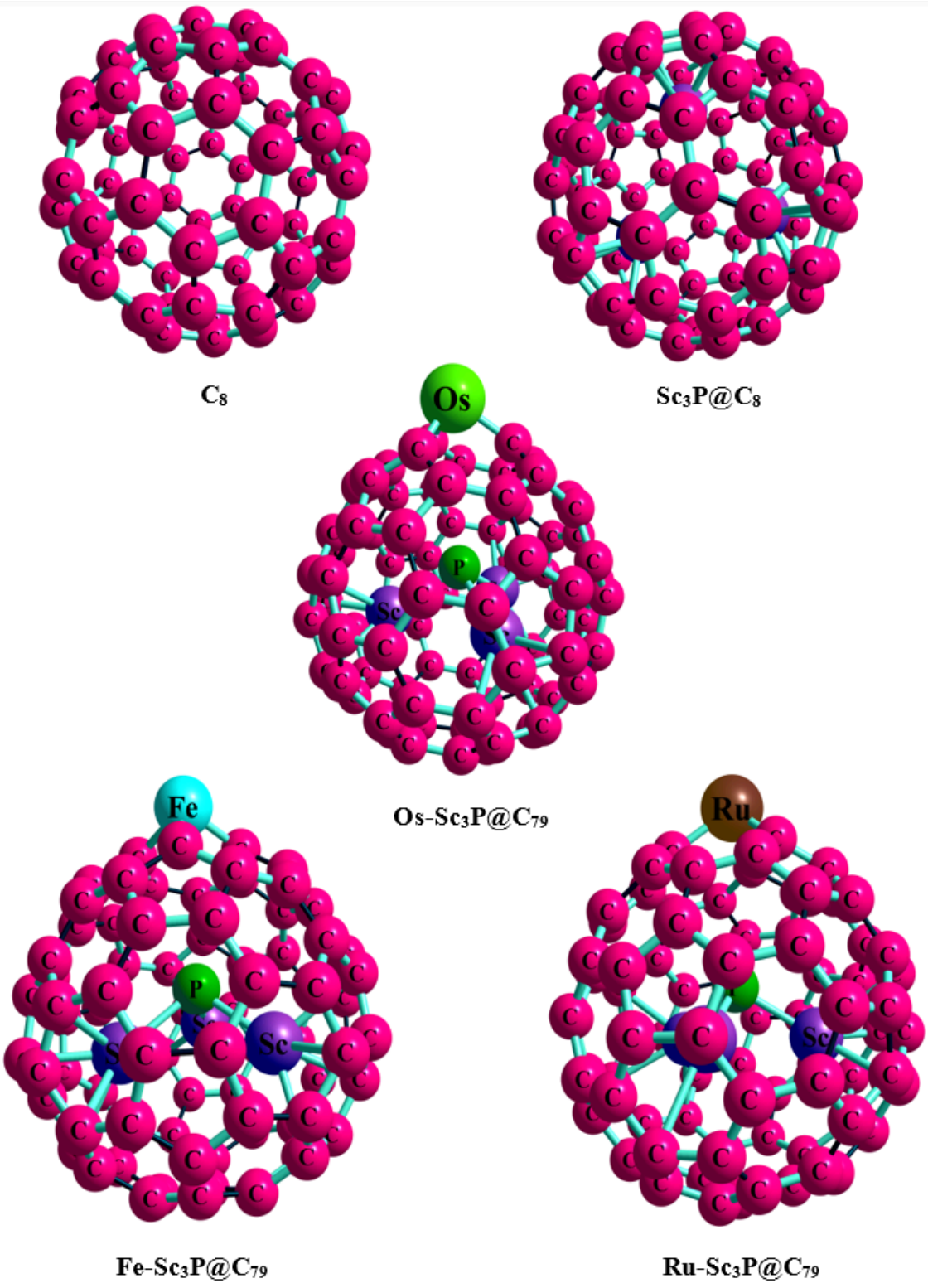


Figure 1

Optimized structures of pristine C_{80}, phosphorus-doped endohedral $Sc_3P@C_{80}$, and transition-metal-doped $Sc_3P@C_{80}$ systems (Fe, Os, and Ru)

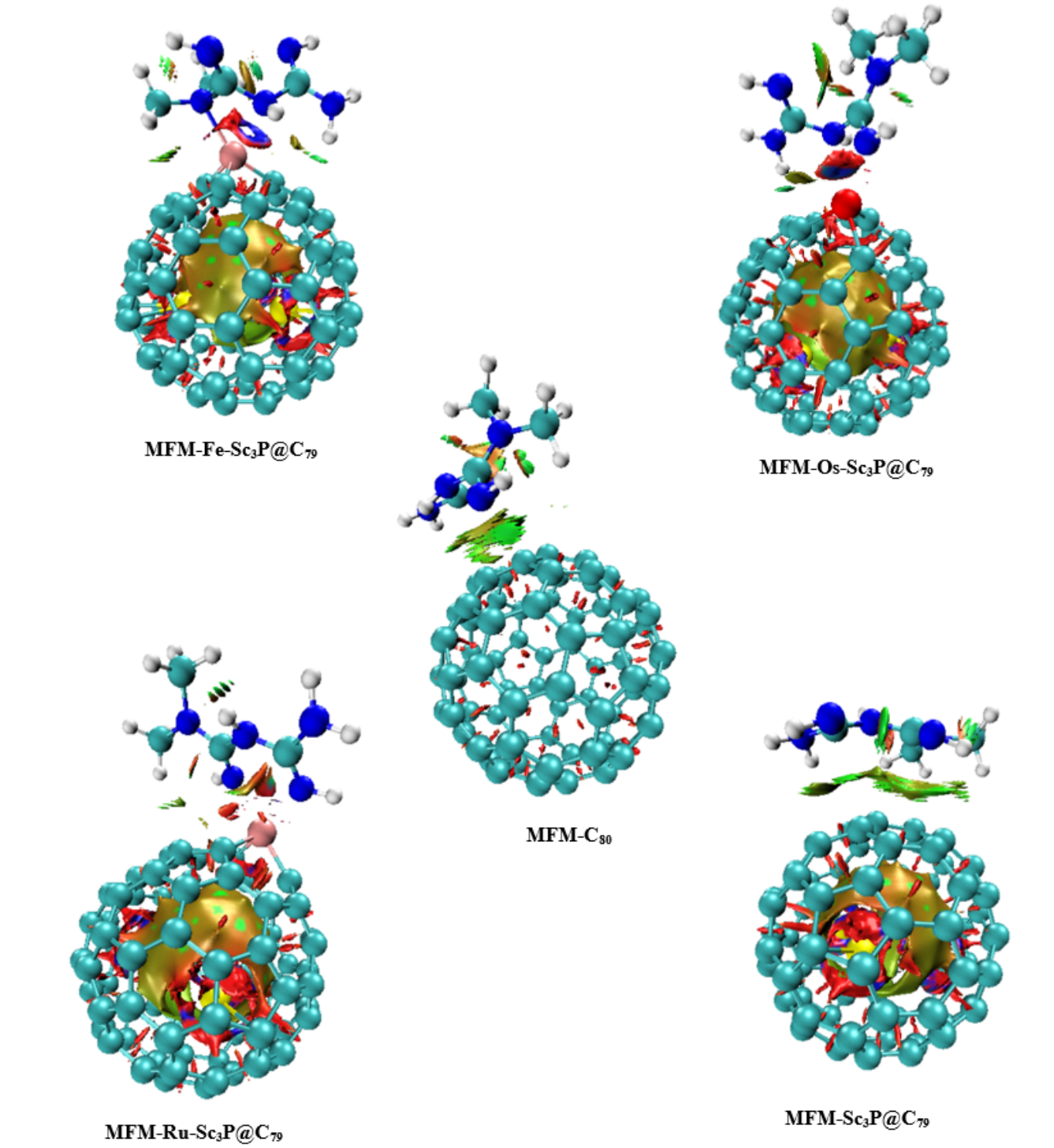


Figure 2

Non-covalent interaction (NCI) isosurfaces for MFM adsorption on pristine and metal-doped Sc_3P@C79 endohedral fullerenes

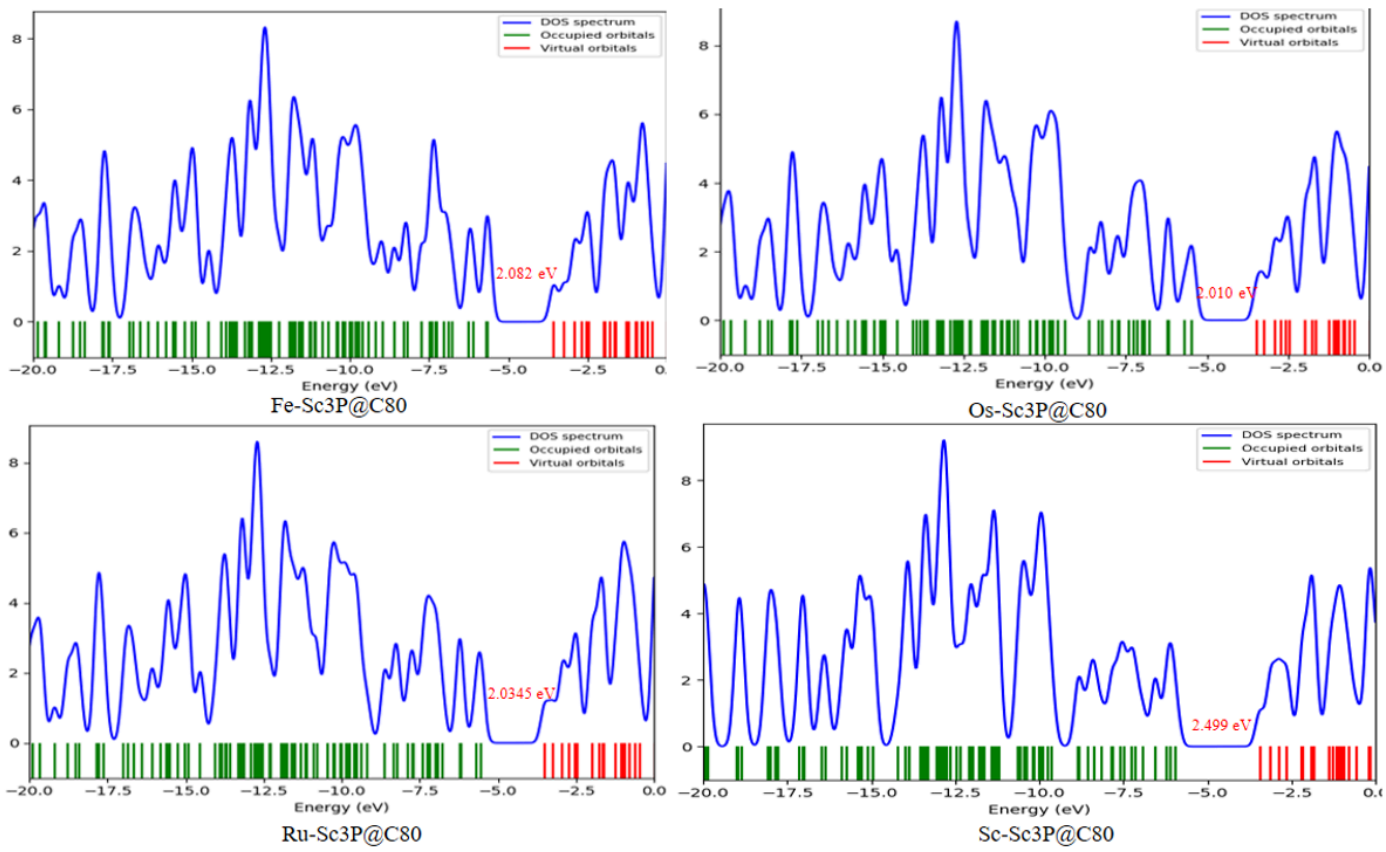


Figure 3

Total density of states (DOS) for Fe–$Sc_3P@C_{80}$, Os–$Sc_3P@C_{80}$, Ru–$Sc_3P@C_{80}$, and pristine $Sc_3P@C_{80}$

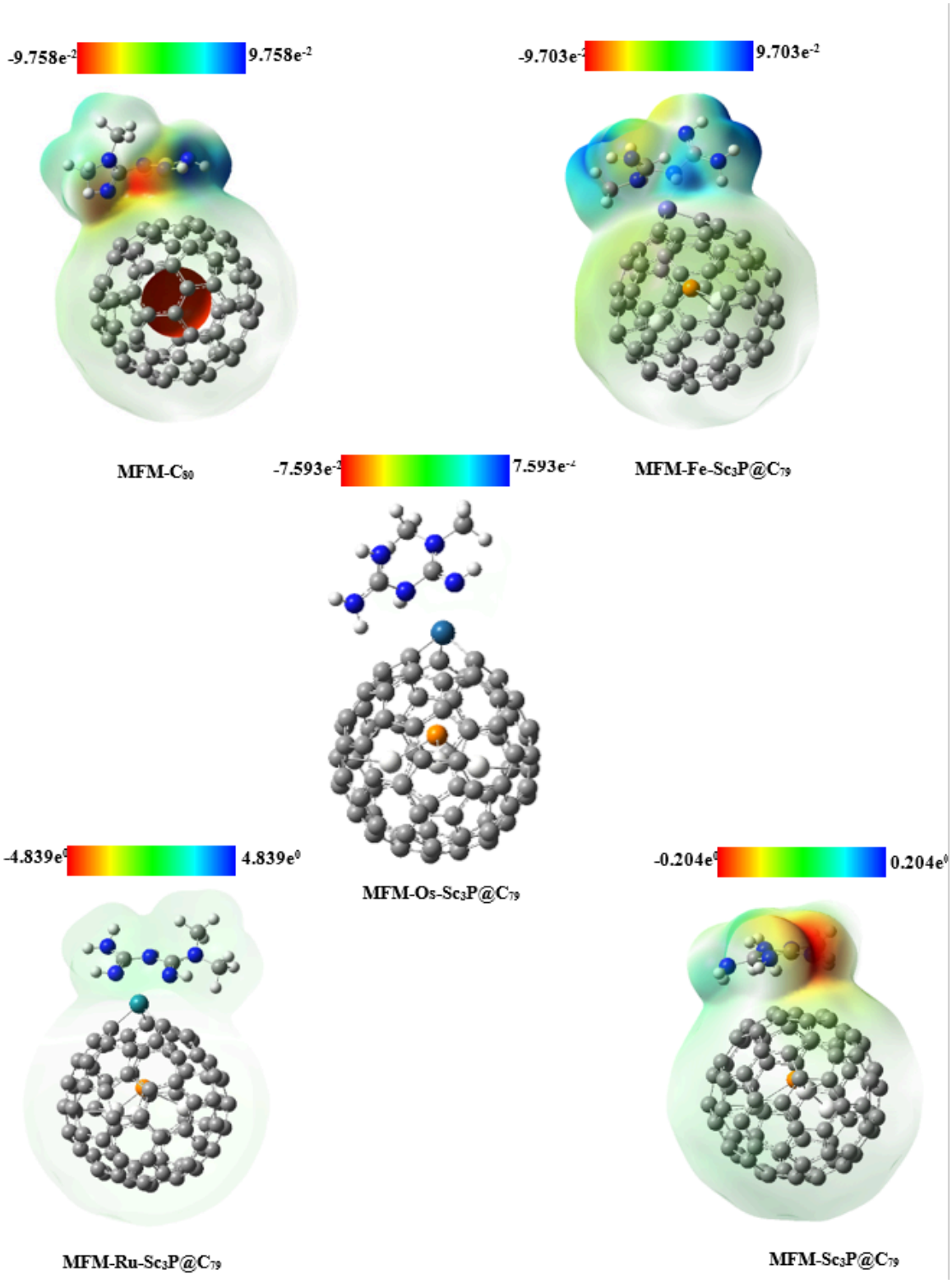


Figure 4

Molecular electrostatic potential (MESP) surfaces of MFM adsorbed on pristine and metal-doped $Sc_3P@C_{80}$ nanostructures: MFM–C_{80}, MFM–Fe–$Sc_3P@C_{79}$, MFM–Os–$Sc_3P@C_{79}$, MFM–Ru–$Sc_3P@C_{79}$, and MFM–$Sc_3P@C_{80}$

Supplementary Files

This is a list of supplementary files associated with this preprint. Click to download.

- MFMsupportingInformation.docx